Membrane mirror characteristics for used with real time holography

Richard A. Carreras, Dan K. Marker, James M. Wilkes

Air Force Research Laboratory, AFRL/DEBS, Kirtland AFB, Albuquerque, NM 87117

ABSTRACT

Space-based inflatable technology is of current interest to NASA, DOD, and in particular to the Air Force Research Laboratory. Potentially large gains in lowering launch costs, through reductions in structural mass and volume are driving this activity. Diverse groups are researching and developing this technology for radio and radar antennae, optical telescopes, and solar power and propulsion applications. Regardless of the use, one common requirement for successful application is the accuracy of the inflated surface figure.

This paper gives a very cursory description of the research being performed at the Air Force Research Laboratory in the fields of membrane mirrors and real time holography. First, the article will show a shape modification method for the membrane mirror, achieved through enforced boundary displacements. The membrane mirror shape modification, resulted in moving the inflated membrane shape towards a desired optical profile. Minimization of the optical figure error is further discussed. Next, the optical requirements levied from the membrane mirror to an optically addressed spatial light modulator performing real time holographic correction are discussed. A proposed optical configuration in which a real time holographic optical element could be combined with the membrane mirror to achieve near diffraction limited optical performance is discussed.

1. INTRODUCTION

Membranes have been studied for many years. There is a great body of literature, which goes back to the 1800's to the early 1900's. This includes the research of Henky and others who have analyzed and evaluated the behavior of membranes[1,2]. The majority of the initial interest was that of analyzing the mathematical elegance and vibration effects of a drumhead [3].

After a brief history of use in space about two decades ago, a resurgence of interest in membrane structures in space is developing. Applications for such structures range from planar configurations in solar sails, concentrators, and shields, to inflatable lenticulars for radar, radio, and optical [4,5,6].

Three key factors are paramount to the success and user acceptance of this technology: deployment, longevity, and performance. For optical application, the performance hinges critically on the precision of the membrane surface coupled with correction mechanisms. The required precision is highly mission dependent, and may entail one or more of the following issues: surface smoothness, deviation from desired surface profile, and slope error. Parabolic profiles are most commonly desired for precision optical telescopes[7]. The most prominent systemic error found in circular inflated or vacuumed membranes is a spherical aberration, often referred to as a "W-profile error"[7,8]. This is a measure of the deviation of the actual surface from that of the desired one.

The Air Force Research Laboratory has recently undertaken the task of creating a large optical quality membrane telescope. The membranes on these telescopes will range in thickness from 20 - 200 micrometers. The maximum acceptable peak-to-peak figure error over the entire surface will range from 10 - 20 micrometers. This value assumes that a certain amount of active optics control will be used to correct surface errors. Part of the Air Force Research Laboratory effort includes methods for achieving the optical precision needed for certain optical applications. Real time holographic techniques using optically addressed spatial light modulators are being considered as the primary optical correction mechanism.

2. DETERMINISTIC SHAPE HISTORY

Let's begin by first reviewing the problem of the inflation of an initially plane, circular membrane, with deformations limited to those that admit only small strains but moderately large rotations. The authors purposefully exclude any consideration of the associated problems of the inflation of annular membranes or circular plates, or of large strain deformation; (see Jenkins and Leonard, 1991, and Jenkins, 1996 for additional details on these topics)[9,10].

This article addresses the investigation of thin membranes with curvature as a primary mirror aperture for use in large optical telescopes. These membrane films are mounted on an optically flat circular ring and stretched over a smaller optically flat circular ring where pressure or vacuum is applied to create the doubly curved surface as shown in Figure 1. The membrane films may vary in thickness from 20 to 200 microns. This particular article examines an aluminum coated

Form SF298 Citation Data

Report Date *("DD MON YYYY")* 00001999	**Report Type** N/A	**Dates Covered (from... to)** *("DD MON YYYY")*

Title and Subtitle Membrane mirror characteristics for used with real time holography	**Contract or Grant Number**
	Program Element Number
Authors	**Project Number**
	Task Number
	Work Unit Number
Performing Organization Name(s) and Address(es) Air Force Research Laboratory AFRL/DEBS Kirtland AFB, Albuquerque, NM 87117	**Performing Organization Number(s)**
Sponsoring/Monitoring Agency Name(s) and Address(es)	**Monitoring Agency Acronym**
	Monitoring Agency Report Number(s)
Distribution/Availability Statement Approved for public release, distribution unlimited	
Supplementary Notes	
Abstract	
Subject Terms	
Document Classification unclassified	**Classification of SF298** unclassified
Classification of Abstract unclassified	**Limitation of Abstract** unlimited
Number of Pages 9	

125 micron thick homogeneous, planar, isotropic membrane with a clear aperture of 28 centimeters. The nature of a flexible membrane implies that the surface curvature will result in an assorted array of gross surface figure issues associated with deterministic shape limits, probabilistic imperfections, nonlinear constitutive effects, and long-time-dependent effects. This article will focus on the empirical deterministic shape limits of a doubly curved membrane. Theoretical work on thin films inflated or evacuated into a doubly curved surface has a long history, and remains an active area of research. A number of articles include summaries of this history, and offer insight on the deterministic membrane shapes[7,8,9,10].

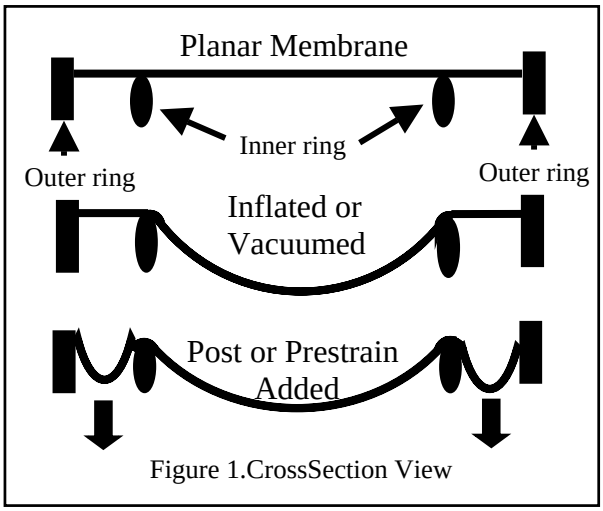

Figure 1.CrossSection View

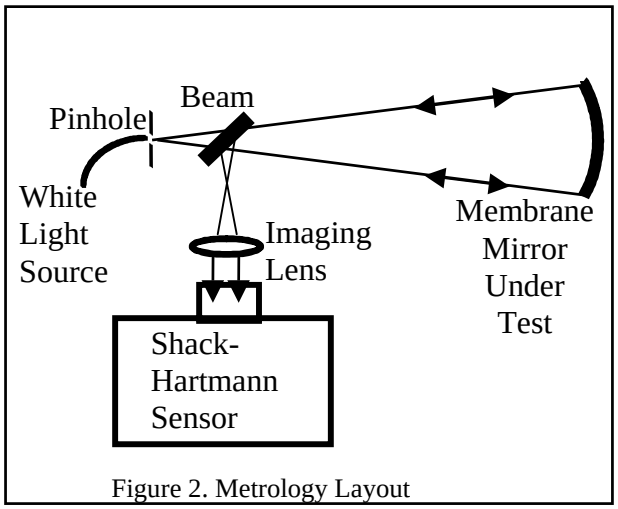

Figure 2. Metrology Layout

The experimental data presented offers precise surface measurement of a 28 cm diameter, 125 um thick polyimide evacuated to form a 4.47 meter concave radius of curvature. Metrology consisted of a Shack-Hartmann wavefront sensor using a 66 by 88 lenslet array with the focal length of each lenslet of 2 millimeters. The angular range of each lenslet is approximately ±17 milliradians. The simple optical layout is shown in Figure 2, but the effort required to take the first set of reliable data was considerable. Measuring a highly aberrated, variable-focal-length optical element is a challenge. The membrane mirror was illuminated at the center of curvature, as shown in Figure 2, and then re-imaged onto a CCD array on the Shack-Hartmann sensor. Any variance from a flat wavefront at the entrance to the lenslet array will be interpreted as a slope error by the Shack-Hartmann sensor. The error represents the difference between the membrane mirror and a perfect sphere. To minimize the influence of the boundary conditions, care must be exercised in the manufacturing of the mounting ring and the membrane mounting process. The outer mounting ring where the film was initially mounted, and the inner ring where the boundary of the doubly curved surface is initiated, were both optically polished to less than 150 nanometers. In addition, a non-symmetric stress state can be introduced if the outer ring is not coplanar with the inner ring. The last significant boundary condition involves the material that slides across the inner ring during a change of curvature, as shown in Figure 1. This change will essentially vary the amount of incremental strain in the material. This incremental strain has a remarkable effect on the optical figure, and it is this strain versus change in optical figure that is the essence of this section.

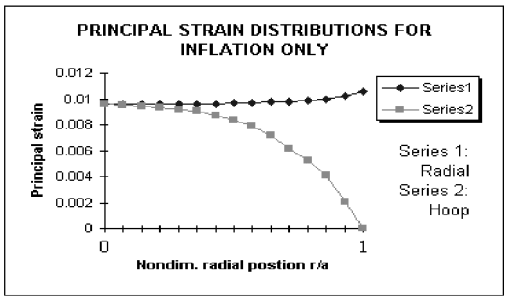

Figure 3. Strain state with ε_i equal to zero

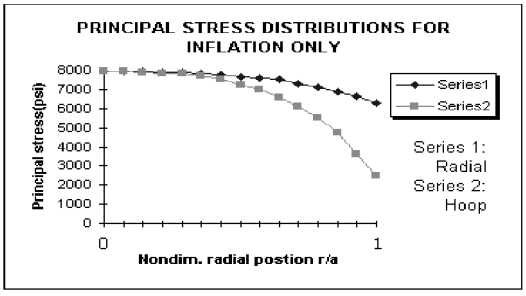

Figure 4. Stress state with σ_i equal to zero

Thus, the object of this exercise is to demonstrate the ability to optically modify the surface figure by varying the amount of incremental strain.

The strain state of the membrane mirror determines the surface optical figure. The stress and strain states that resulted from the uniform pressure applied during evacuation are shown in Figures 3 and 4. These stress and strain distribution to a clamped boundary membrane are denoted as σ_e and ε_e respectively. As long as in-plane compressive forces are not imposed, incremental stress and strain can be added to or subtracted from the membrane film via symmetric and continuous in-plane radial forces. This reasonably assumes a frictionless contact at the inner ring because the boundary exhibits no noticeable friction when compared to the movements required to make even small changes in the incremental strain. Incremental stress and strain is now defined as σ_i and ε_i respectively. The order in which the incremental and evacuation stresses are imparted is irrelevant. Thus, incremental stress can be added in full or in parts before or after curvature is initiated and the final surface figure will be identical. The terms prestrain and poststrain, respectively, are used to identify incremental strain added or removed, respectively, from the membrane film. Prestrain is the ε_i added when the membrane is planar and poststrain is the ε_i added or removed after curvature is initiated.

Figure 5 shows the mirror in the planar mode with co-author Dan Marker and, in Figure 6, a vacuum is applied to both the annulus and the inner cavity. The magnification is produced by the concave curvature of the center portion of the membrane mirror being evacuated while the outer effect is produced by the concave curvature of the annulus, which is controlled by a separate vacuum pump. Changes in the annulus curvature will increase or decrease the incremental strain imparted to the central membrane.

Figure 5. Flat membrane

Figure 6. Vacuumed using edge control

Care must be exercised in maintaining the boundary conditions of the evacuated membrane and in tracking the radial migration of material across the inner ring. Consider how the effects of mounting technique(ε_i), annulus curvature(ε_i), and the strain(ε_e) added due to the curvature of the central membrane, will contribute to the overall strain state. First, strain added during the mounting process is shown in Figure 7. As the outer ring is translated a distance *l*, prestrain will be imparted. The strain distribution near the outer ring is highly nonlinear but the distribution within the inner ring is approximately constant. Second, additional prestrain can be added by varying the radius *r* shown in Figure 8.

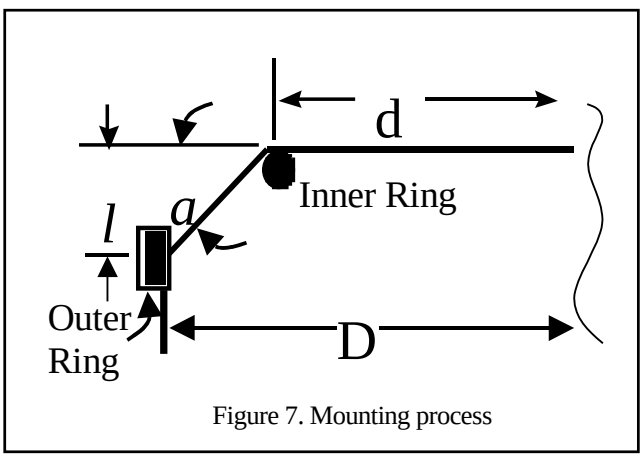

Figure 7. Mounting process

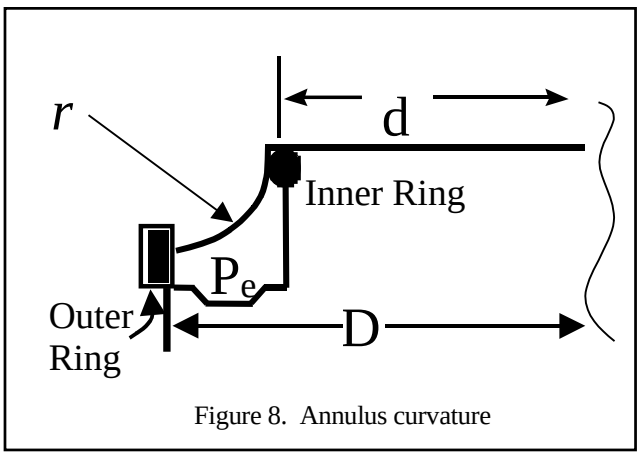

Figure 8. Annulus curvature

This is accomplished by an independent vacuum pump connected to the annulus cavity. This action will pull material radially outward across the inner ring when the vacuum is increased and allow material to migrate inward when the vacuum is decreased. Third, strain is now added by evacuating the inner ring cavity as shown in Figure 9. Recall, this stress (strain) distribution of a clamped boundary membrane which were shown in Figures 3 and 4. Adding curvature will result in a reduction of prestrain. A deeper curvature will increase the radial stress at the boundary so that the force equilibrium of the annulus material is upset. Consequently a certain amount of material will migrate radially inward across the inner ring. Recall that the net effect of allowing material to radially cross the inner ring at any time before or after inner ring curvature is initiated is to simply modify the incremental strain of the central membrane. Thus, increasing the central curvature will reduce the amount of prestrain initially imparted to the membrane. With the correct amount of prestrain added during the mounting process, one can achieve a zero prestrain condition for any given curvature (as shown on Figure 10).

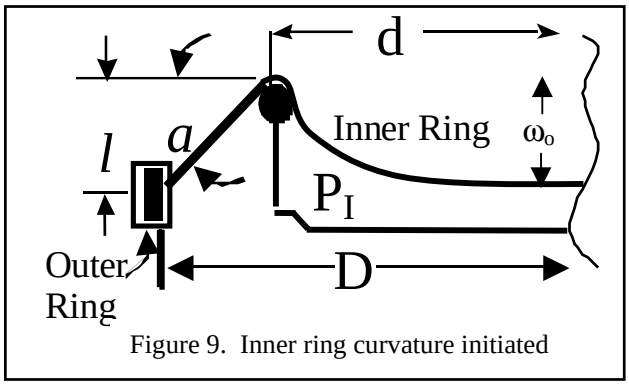

Figure 9. Inner ring curvature initiated

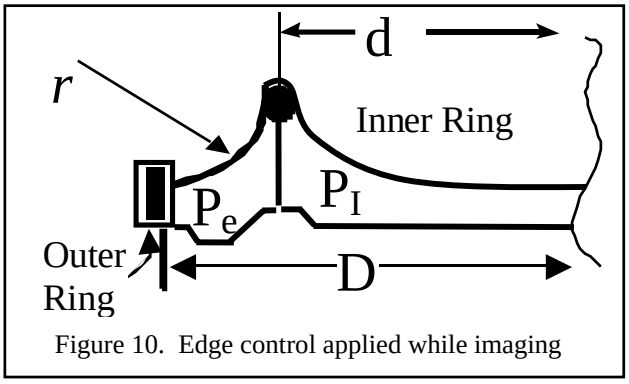

Figure 10. Edge control applied while imaging

Examining the surface figure of a membrane mirror of radius r_0 = 14 *cm* and thickness t = 125μ*m*, characterized by a Young's modulus E = 8800 N/m^2, and a Poisson's ratio ν = 0.4. Consider its response at two different inner cavity pressure differentials P_t , viz., 2.0 and 7.3 inches of water, and a central deflection of ω_0 = 2.18 *mm* (corresponding to an optical system with f-number of 8) at each of these pressures.

Based on a theory presented by Campbell[11] (modified by extending his power series expansion for the lateral deflection $\omega(r)$ to include eleven rather than six terms, and computing the expansion coefficients for a Poisson's ratio of 0.4 rather than 0.3. Now the prestrain necessary to accomplish this central deflection at the two pressure differentials can be determined. Campbell's theory is applicable to a membrane subject to an initial tension σ_i, related to an initial strain (prestrain) ε_i by

$$\sigma_i = \frac{E}{1-\nu}\ \varepsilon_i . \tag{1}$$

For zero prestrain, the theory yields the following expression for the central displacement:

$$\omega_0 = 0.626\, r_0 \left| \frac{P_e\, r_0}{E\, t} \right|^{1/3} \tag{2}$$

cf., Campbell's equation (25), where the difference in numerical factors is due mainly to the different Poisson's ratios[11]. This can be solved for the pressure P_e required to produce the displacement, yielding

$$P_e = 4.076 \left| \frac{\omega_0^{\,3}}{r_0^{\,4}} \right| Et \tag{3}$$

On the other hand, for *large* values of initial tension (or prestrain), Campbell's theory yields the following expression for the central displacement:

$$\omega_o = \frac{1}{4} \left| \frac{r_0^{\,2}}{\sigma_i t} \right| P_i \tag{4}$$

cf., his equation (26). From this we obtain the following expression for the pressure P_i required to produce a displacement ω_0 of a membrane under large prestrain:

$$P_i = 4 \left| \frac{\omega_0}{r_0^{\,2}} \right| \sigma_i t = 4 \left(\frac{\omega_0}{r_0^{\,2}} \right) \left(\frac{Et}{1-\nu} \right) \varepsilon_i \tag{5}$$

In the last equation, (1) was used to write the result in terms of the prestrain rather than the initial tension. We find that the total pressure P_t required to maintain the displacement ω_0 for a given value of prestrain is very well estimated by the sum of the two pressures given in (3) and (5), i.e., by the linear function

$$P_t = P_e + P_i = 4.076\left|\frac{\omega_0^4}{r_0^4}\right| Et + 4\left(\frac{\omega_0}{r_0^2}\right)\left(\frac{Et}{1-\nu}\right)\varepsilon_i \tag{6}$$

Substituting the appropriate values for the constants, we obtain in units of inches of water:

$$P_t = 0.5 + 32.9\varepsilon_i \tag{7}$$

where the prestrain is given as some percent of the radius r_0. This can be solved for the prestrain to obtain

$$\varepsilon_i = \frac{P_t - 0.5}{32.9} \tag{8}$$

Thus, from this formula we find 0.05% and 0.21% for the required prestrains at pressure differentials of 2.0 and 7.3 inches of water, respectively, in order to produce a central deflection of 2.18 *mm*.

The Campbell theory can subsequently be used to determine for a given prestrain the maximum deviation of the membrane from, for example, a reference sphere. This deviation is a measure of the maximum amount of spherical aberration to be expected. In Figure 11 The authors have plotted the results for the maximum deviation of the membrane from an f-number of 8, reference sphere, in waves of λ = 633 *nm* light, as a function of the percent prestrain. For the two prestrains just calculated, we obtain from this curve values of 25λ and 7λ, which are indicated in Figure 11.

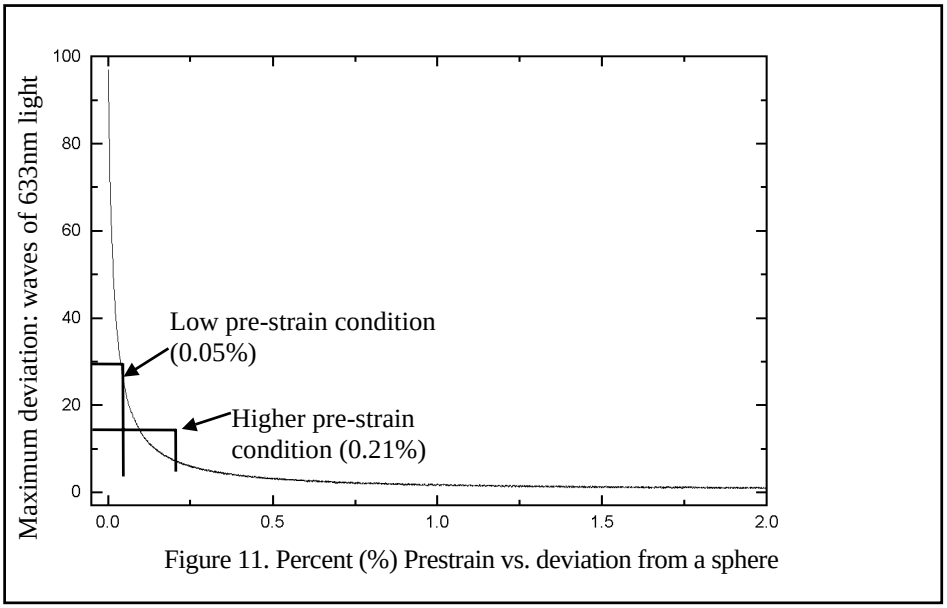

Figure 11. Percent (%) Prestrain vs. deviation from a sphere

3. SPATIAL LIGHT MODULATOR RESOLUTION REQUIREMENTS

It has always been assumed that the membrane mirrors will have very large optical aberrations. The key to getting the membrane mirror to operate as an optical reflector is the ability to correct for these large optical aberrations. Therefore, as a first step, it is important to fully optically characterize the membrane mirror. In addition, it is necessary to analyze the magnitude of the aberrations and the angular deviation from a desired shape to see if these measurements are within the range of correction for an optically addressed spatial light modulator used as a real time holographic correction element.

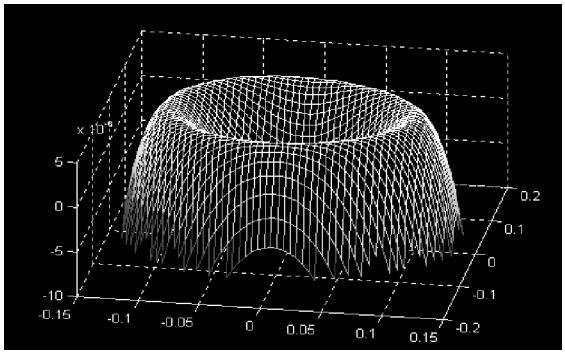

Figure 12.Estimated surface at full aperature & lower pressure.

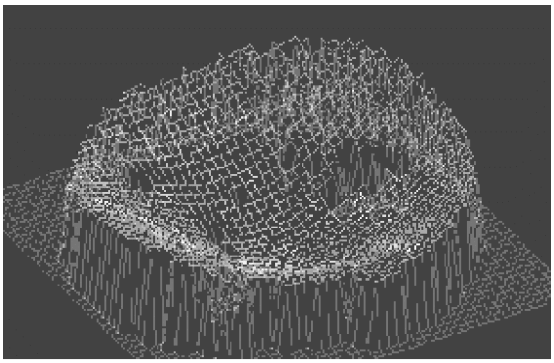

Figure13.Central 183 mm of aperture shown in Fig 12.

The Shack-Hartmann interferometer was chosen as the optical diagnostics tool to measure the optical characteristics of the membrane mirror. Two data sets will describe the mirror's optical figure; one at the full aperture of 280 millimeter diameter, and one when the aperture is stopped down to 183 millimeter diameter. The Shack-Hartmann sensor is driven out of range when the entire aperture is viewed at the low central pressure. In this case, the estimated surface quality is derived from a model based upon Hartmann sensor data for the central 183 mm and an interpretation of the Foucalt test data for the full aperture. The vacuum pressure is set at 2 inches of water for both Figure 12 and Figure 13. Figure 12, the estimate for the full aperture, shows a total spherical aberration of 15 waves, while the central 183 millimeters in Figure 13 (the actual measurement) shows 8.5 waves of spherical aberration. Figure 12 is the only data set that is estimated. Again, the estimation was necessary since the aberrations of the full aperture, low pressure case, were out of range of the Shack-Hartmann sensor. All other measurements were taken directly from the Shack-Hartmann sensor.

The surface measurement for the stopped-down aperture in Figure 13 and Figure 15 were taken to give the reader a direct comparison of an actual measured portion of the membrane at two different pre-strain conditions. The results clearly show the effects of the two different incremental strains.

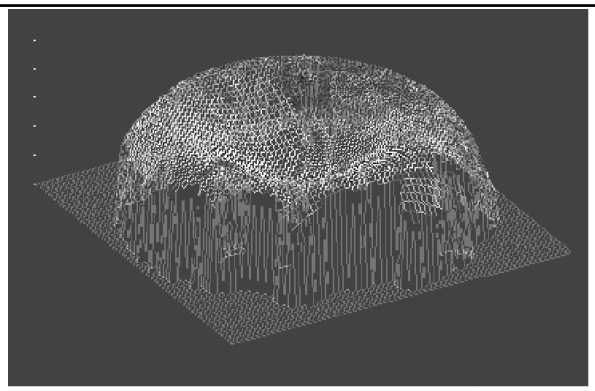

Figure14.Measured surface at full aperture & high pressure.

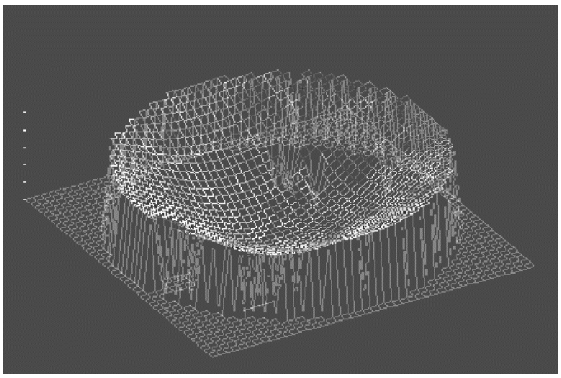

Figure15.Central 183 mm of aperture shown in Fig 14.

The full aperture shown in Figure 14 has a total spherical aberration of 5.5 waves across the entire 280 mm aperture. Vacuum pressure is set at 7.3 inches of water. The dropouts near the edge are due to an out-of-range condition in the Hartmann sensor. Figure 15 is the Hartmann sensor data for the central 183 mm of the full aperture shown in Figure 14. The surface aberration, in Figure 15, is due to a spherical aberration of 3.5 waves.

The measured spherical aberration for the two pressure data points and the associated spherical aberration calculated using Campbell's results are summarized in the following table. Note that the theoretical and experimental spherical distortions are in very good agreement. Compare the spherical aberration for the 183 millimeter aperture and one immediately sees a similar trend. The measured results are within 40% of that calculated for the low pressure, and within 22% of calculated for the high pressure.

Differential Pressure Inner Ring (Inches of H_2O)	Calculated Incremental Stain (Prestrain) (%)	Calculated Surface Deviation (waves @ 633um) Full Aperture	Measured Surface Deviation (waves @ 633um) Full Aperture	Estimated Surface Deviation (waves @ 633um) Full Aperture	Measured Surface Deviation (waves @ 633um) Central 183mm
2.0	0.05	25	n/a	15	8.5
7.3	0.21	7	5.5	n/a	3.5

Table 1. Summary of theory vs experimental results (when compared to a sphere)

Clearly there is a strong correlation between theory and the laboratory results. More importantly, the authors are able to experimentally prove the idea of adding prestrain to manipulate the surface quality at optical tolerances. Essentially, the more prestrain that is added to a membrane the more spherical the shape will become. It is not possible, with our present techniques, to create a parabolic surface from a planar homogeneous, isotropic uniform thickness membrane mounted onto a planar circular ring. A sphere is the mechanical limit, which implies that $\varepsilon_i >> \varepsilon_e$. As the nonlinear strain becomes dominant the geometry of the outer 1/3 of the membrane's aperture becomes more oblique. So as the optical figure diverges from a sphere the divergence from a parabolic shape becomes even greater.

When membrane mirrors are considered as an optical element for use with real time holography, two important issues must be considered. The first issue is the fringe density within the range of the optically addressed spatial light modulator (OASLM). The second issue is the fringe velocity, and whether the fringe velocity can be tracked by the OASLM. This second issue could be looked at as the frequency response bandwidth of the OASLM. This article will address the magnitude of the fringe density and leave the fringe velocity issue as a follow on topic.

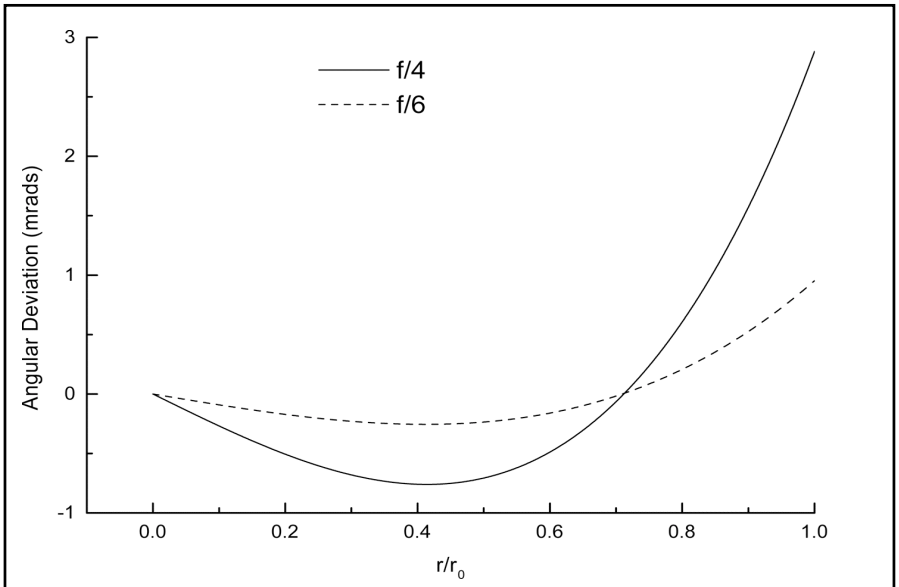

Figure16.Angular Deviation with respect to radius for an f /4 and f /6 mirrors

Fringe density is directly related to the angular deviation of the membrane mirror when compared to some reference surface. This reference wave could either be spherical or parabolic depending on the optical setup and the application. If the angular deviation is too great then the OASLM will not have the resolution needed to correct for the aberration[14]. Therefore, a modeling effort was undertaken to understand these requirements of the membrane mirror and what it meant to the application of an OASLM.

Figure 16 shows how the angular deviation changes from the center of the membrane mirror as it goes out radially toward the outer ring. The horizontal axis is $\mathbf{r/r_o}$, where $\mathbf{r}$ is the fixed radius of the membrane mirror and $\mathbf{r_o}$ is a variable starting at the center and going out radially toward the rim. Thus, as the variable $\mathbf{r_o}$ reaches the radius $\mathbf{r}$, then $\mathbf{r/r_o}$ becomes one (1.0), as seen in Figure 16. As can be seen, the maximum angular deviation from a spherical reference occurs at the edge. Figure 16 shows the results for a membrane mirror deformed to an f-number of 4, (f/4). A maximum angular deviation of 3 milliradians is calculated. As expected, as the f-number is relaxed the angular deviation is reduced, i.e. for an f-number of 6, (f/6), a maximum angular deviation of 1 milliradians is calculated (as shown in Figure 16).

Thus, the next logical step was to investigate the behavior of the angular deviation with respect to f-number. This is shown in Figure 17. As evident from Figure 16 the maximum deviation is always shown to occur at the edge of membrane mirror. Thus, this is the single position of the measurement of the angular deviation for Figure 17. As the f-number gets larger the curvature of the mirror is less, thus, the membrane mirror's angular deviation is also less. The three curves shown in Figure 17, depicts the reduction of angular deviation as the clear aperture is reduced via an aperture stop. Stopping down the aperture diameter by 10% reduces the angular deviation by almost 50%. From our previous research, it has been found that the membrane better approaches a perfect mirror in the center, and deviates from the perfect mirror as the radius is increased toward the rim[7,8,12]. Efforts to further improve this behavior are in process but for a planar,

isotropic, homogeneous, even thickness membrane with .25% prestrain the performance will remain as shown in Figure 17.

The scalability of the membrane and associated aberrations and angular deviation is also of great importance. The magnitude of the aberration does indeed increase as the size of the membrane mirror gets larger. This increase has been documented in several other articles from this group[7,8,13]. What the authors would like to report here is that the angular deviation stays constant and does not change as the membrane gets larger. This fact is of great interest and will be experimentally verified in the near future.

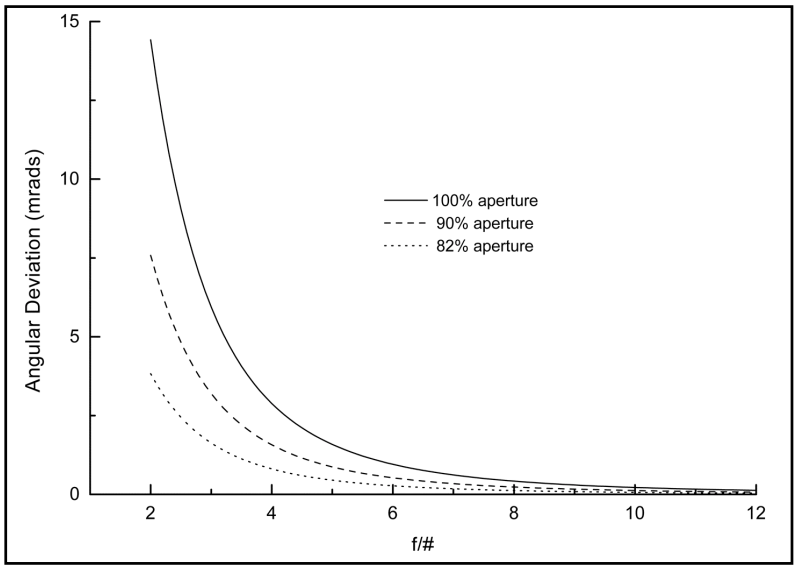

Figure 17. Angular deviation with respect to aperture fill factor.

4. POSSIBLE MEMBRANE MIRROR - OASLM SETUP

As seen from the previous sections, the aberrations from the membrane mirror can be severe. These aberrations are typically too large to be corrected by conventional wave front correction techniques, which use deformable mirrors.

The dynamic range of the OASLM has been demonstrated to correct for hundreds of waves of distortions[14]. This large dynamic range will be of increasing importance, as more aggressive large, lightweight mirror designs are demanded. Apertures larger than 4 meters will most likely be deployed. Thus, structural rigidity will be more difficult to control, and there will be additional dynamic optical aberrations. The addition of mechanical and active damping will diminish the weight savings, thus, the correction task will shift to small lightweight optical device such as OASLM's.

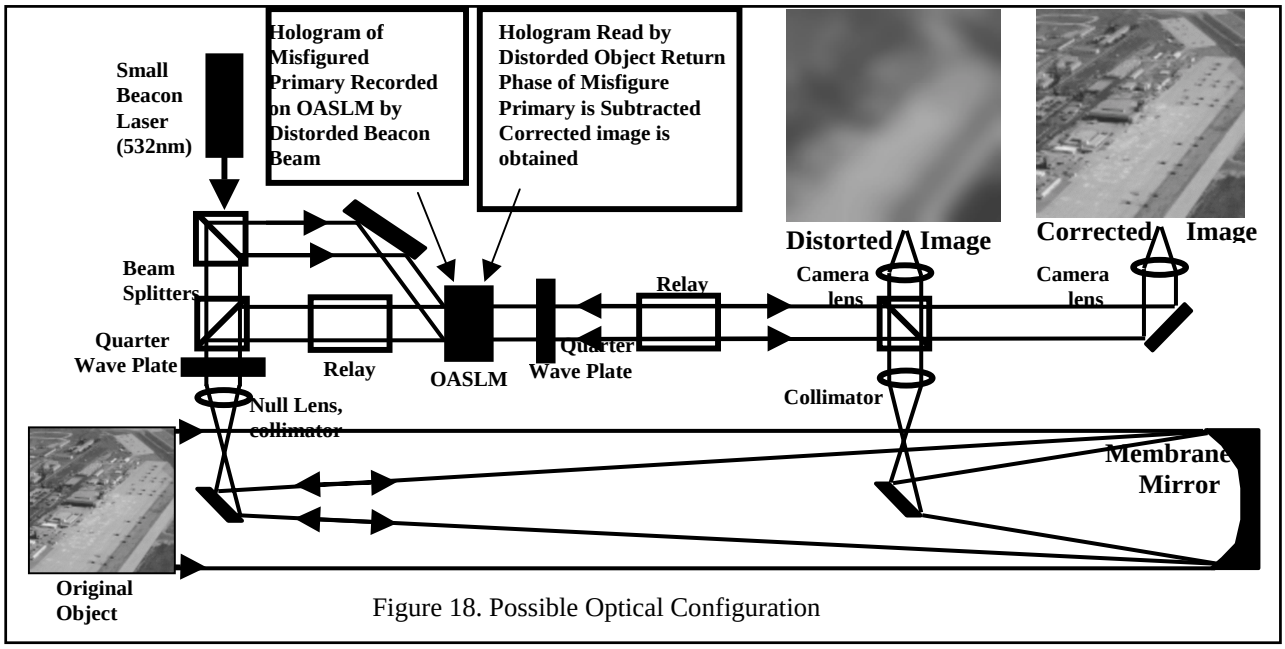

Figure 18. Possible Optical Configuration

Given the possibility that membrane mirrors can be corrected using a real time holographic device, various possible optical configurations have been considered. The first is to use an optical configuration, which has been used at the Air Force Research Laboratory in testing a variety of real time holographic devices. Figure 18 shows an OASLM used to perform real time holographic optical correction. The membrane mirror is shown as the large, primary aperture for a telescope used in an imaging application. The membrane mirror is also the source of all the optical aberrations in the optical system. The distorted image is shown next to the corrected image. A beacon laser is shown probing the membrane mirror, and later mixed with the image beam at the OASLM. The OASLM then produces the corrected image.

5. CONCLUSIONS

The Air Force Research Laboratory has undertaken the task of proving that membrane mirrors can be used as large, high quality optical mirrors. This task was divided into two separate lines of research. The first line of research involved investigating the membrane mirror and understanding if there are any means of improving it's optical characteristics. The second line of research involved utilizing the long history of the Air Force Research Laboratory in applying adaptive/active optical correction techniques to correct for the residual aberrations in an optical system. Basically, this means looking at different adaptive/active correction techniques having very large dynamic ranges. The hope was that in attacking this problem from both ends, i.e. improving the membrane mirror and increasing the dynamic range of adaptive/active correction, a solution could be found somewhere in the middle.

The first half of this article describes the results and methods use by the authors in attacking the first line of research, i.e. improving the optical quality of the membrane mirror. A small amount of theory and several significant results were discussed. The last part of this article shows how the authors have converged on real time holography as the adaptive/active optical correction of the residual aberrations. The membrane mirror data, which is taken, was examined for the explicit purpose of understanding whether the OASLM could perform the optical correction of the membrane mirror residual aberrations.

The match between the membrane mirror and the OASLM performing real time holographic correction seems to be appropriate. Finally, an optical setup, which uses an OASLM for correcting the membrane mirror aberrations, is proposed.

6. REFERENCES

1. Hencky, H. (1915), "Uber den Spannungszustand in kreisrunden Platten," *Z. Math. Phys*. 63, 311-317.
2. Föppl, A. (1907), "Vorlesungen uber technische Mechanik," *B.G. Teubner*, Bd. 5., p. 132, Leipzig, Germany.
3. J.W.S. Rayleigh, "Theory of Sound, Vol.1 & Vol.2", New York, New York, Dover Publications, 1945
4. Grossman, G., and Williams, G. (1990). "Inflatable concentrators for solar propulsion and dynamic space power," *J Solar Energy Engineering* **112**, 229-236.
5. Hart-Smith, L.J., and Crisp, J.D.C. (1967), "Large elastic deformations of thin rubber membranes," *Int J Eng Sci* **5**, 1-24.
6. Hedgepeth, J.M. (1982), "Accuracy potentials for large space antenna reflectors with passive structures," *J Spacecraft* **19**(3), 211-217.
7. Marker, D. K. and Jenkins C. H., "Surface precision of optical membranes with curvature," *Optics Express vol 1, no 11, pg 301-362*, www.osa.org, Nov. 24, 1997.
8. Jenkins, C.H., Marker, D.K., and Wilkes, J.M., "Improved surface accuracy of precision membrane reflectors through adaptive rim control," *AIAA Adaptive Structures Forum*, Long Beach, CA (1998).
9. Jenkins, C.H., "Nonlinear Dynamic Response of Membranes: State of the Art -- Update," *Appl Mech Rev 49 (10), S41*-S48 (1996).
10. Jenkins, C.H., and Leonard, J.W., "Nonlinear Dynamic Response of Membranes: State of the Art," *Appl Mech Rev 44, 319-328* (1991).
11. Cambell, J.D., "On the theory of initially tensioned circular membranes subjected to uniform pressure," *Q J Mech Appl Math* **9**, 84-93 (1956).
12. Wilkes, J. Technical in preparation, 1998
13. Jenkins C.H. and Marker D. K., Journal of Solar Energy Engineer
14. M. T. Gruneisen, K. W. Peters and J. M. Wilkes, "Compensated Imaging by Real-Time Holography with Optically Addressed Spatial Light Modulators," Proceedings from the SPIE 42nd Annual Meeting, San Diego, CA, July 27-August 1, 1997, Paper 3143-25.